

# 1 **Investigation of cosmic ray–cloud connections using MISR**

2 Joshua Krissansen-Totton and Roger Davies

3 Department of Physics, The University of Auckland, Auckland, New Zealand

4 Numerous empirical studies have analyzed International Satellite Cloud Climatology  
5 Project (ISCCP) data and reached contradictory conclusions regarding the influence  
6 of solar-modulated galactic cosmic rays on cloud fraction and cloud properties. The  
7 Multiangle Imaging SpectroRadiometer (MISR) instrument on the Terra satellite has  
8 been in continuous operation for 13 years and thus provides an independent (and  
9 previously unutilized) cloud dataset to investigate purported solar–cloud links.  
10 Furthermore, unlike many previous solar–climate studies that report cloud fraction  
11 MISR measures albedo, which has clearer climatological relevance. Our long-term  
12 analysis of MISR data finds no statistically significant correlations between cosmic  
13 rays and global albedo or globally averaged cloud height, and no evidence for any  
14 regional or lagged correlations. Moreover, epoch superposition analysis of Forbush  
15 decreases reveals no detectable albedo response to cosmic ray decreases, thereby  
16 placing an upper limit on the possible influence of cosmic ray variations on global  
17 albedo of 0.0029 per 5% decrease. The implications for recent global warming are  
18 discussed.

## 19 **1. Introduction**

20 The analysis of paleoclimate records has uncovered numerous robust correlations  
21 between climate proxies and indicators of solar activity [*Bond et al.*, 2001; *Neff et al.*,

22 2001]. Although current knowledge of long-term variations in total solar irradiance  
23 (TSI) is incomplete, arguably these close correlations cannot be fully explained by  
24 changes in globally averaged TSI alone [Kirkby, 2007]. This suggests the existence of  
25 some indirect solar influence on Earth's climate that amplifies relatively small  
26 changes in TSI.

27 Two broad categories of mechanisms have been proposed to explain observed  
28 solar-climate connections: indirect irradiance mechanisms [e.g. Haigh, 1996; Meehl  
29 *et al.*, 2009] and solar-modulated cosmic ray (CR) mechanisms, the latter being the  
30 focus of this study. During times of high solar activity, the sun's intensified magnetic  
31 field sweeps away galactic CRs from within the solar system, thus reducing the CR  
32 flux recorded on earth and ensuring the CR flux and solar activity are negatively  
33 correlated [Bazilevskaya *et al.*, 2008]. It has been argued that solar-modulated  
34 variations in CRs may in turn alter cloud properties via modulation of the global  
35 electric circuit [Tinsley, 2008] or changes in CCN formation [Marsh and Svensmark,  
36 2000]. The prediction of the latter hypothesis is that increasing the CR flux increases  
37 atmospheric ionization, which in turn leads to higher CCN populations and therefore  
38 higher albedos. Unfortunately it is difficult to distinguish between competing  
39 mechanisms from observations alone since all indicators of solar activity such as  
40 CRs, TSI, sunspot number and the UV flux are all closely correlated [Gray *et al.*,  
41 2010]. However despite this causal ambiguity it is helpful to determine whether and  
42 to what extent solar-climate correlations exist as a stepping-stone to understanding  
43 potential mechanisms.

44 Various empirical studies have claimed strong correlations exist between galactic  
45 CRs and satellite-detected cloud cover on interannual timescales [e.g. *Svensmark and*  
46 *Friis-Christensen, 1997; Pallé and Butler, 2000; Marsh and Svensmark, 2003*]. From  
47 these correlations it has been argued that the radiative forcing due to galactic CR  
48 modulation of cloud fraction could potentially explain most of the global warming  
49 observed in the 20th century [*Svensmark, 2007; Rao, 2011*]. However the choice of  
50 data and methods of analysis in these correlational studies have been heavily  
51 criticized [e.g. *Jorgensen and Hansen, 2000; Damon and Laut, 2004*], and similar  
52 empirical analyses by *Kristjansson et al. [2004]* and *Sun and Bradley [2002]* have not  
53 supported a galactic CR–climate link.

54 An alternative approach for investigating links between solar activity and climate is  
55 the epoch superposition of Forbush decreases (see references below). Forbush  
56 decreases (Fds) are sudden decreases in the surface CR flux caused predominantly  
57 by coronal mass ejections. The decrease takes place over several hours whilst the  
58 recovery back to original levels may take several days. By superposing multiple Fds  
59 and comparing their composite to a cotemporal superposition of atmospheric data it  
60 is possible to test whether sudden decreases in CRs are correlated with an  
61 atmospheric response. Since Fds are comparable in magnitude to CR variation over  
62 the 11-year solar cycle, purported correlations between CRs and climate on  
63 interannual timescales may also be apparent during Fds. Furthermore the short  
64 timescales involved allow internal modes of variability to be excluded as competing  
65 explanations for any correlations or trends.

66 Numerous composite studies have investigated possible atmospheric responses to  
67 Fds with positive results [e.g. *Pudovkin and Veretenenko*, 1995; *Todd and Kniveton*,  
68 2001, 2004; *Svensmark et al.*, 2012]. However many similar studies have obtained  
69 results consistent with the null hypothesis [e.g. *Kristjansson et al.*, 2008; *Sloan and*  
70 *Wolfendale*, 2008; *Calogovic et al.*, 2010; *Laken and Calogovic*, 2011].

71 Part of the reason why definitive results have proven elusive is because the majority  
72 of existing satellite-based studies are not independent; with the exception of a small  
73 number of studies that utilized MODIS, almost all empirical solar–climate studies  
74 have relied on ISCCP. The over-reliance on a single dataset is problematic because  
75 there are artefacts within the ISCCP dataset that arguably make it unsuitable for  
76 long-term analysis [*Laken et al.*, 2012 and references therein]. The MISR instrument  
77 on the Terra satellite has been in continuous operation for 13 years and thus  
78 provides an independent and well-calibrated cloud dataset for investigating both  
79 long-term and short-term connections between CRs and climate. To our knowledge  
80 this study is the first time MISR has been used to explore solar–climate links.

## 81 **2. Data**

82 CR data were obtained from the Neutron Monitor Database (NMDB). For the long-  
83 term analysis, CR time series with daily count rates from eight different monitoring  
84 stations were anomalized, scaled by their own variances, and averaged to produce a  
85 13-year CR composite to represent the normalized global CR flux (see  
86 supplementary material for list of monitoring stations).

87 Albedo and cloud height data were obtained from the MISR dataset. MISR utilizes 9  
88 multi-channel cameras positioned at different viewing angles; this allows cloud-top  
89 heights to be stereoscopically derived, and top-of-atmosphere albedos to be inferred  
90 by integrating bidirectional reflectance factors over all 9 zenith angles and modeling  
91 azimuthal angle dependency [*Diner et al.*, 1999]. Thus MISR's 'expansive' albedo  
92 measurements mimic what an albedometer would measure if placed 30km above  
93 the surface. By comparison, ISCCP albedo estimates involve modeling of both  
94 azimuthal and zenith directionality and only attempt to determine the albedo at the  
95 top of the local reflecting layer. Although azimuthal directionality must still be  
96 modeled in MISR's case, the main result is differential so biases due to modeling  
97 cancel out [*Diner et al.*, 1999]. We analyzed the entire MISR dataset of expansive  
98 albedo values and zero-wind reflecting layer reference altitudes values (cloud-top  
99 height) available from the level 2 processing for the time period April 2000 to  
100 February 2013. These data were initially summarized in 140km along-track by  
101 380km across-track 'blocks'. There are 180 blocks per orbit and MISR completes  
102 14.56 orbits per day.

103 Many of the solar-climate studies referenced above have focused on cloud fraction  
104 as opposed to albedos, which are the subject of this study. The advantage of using  
105 albedos to study solar-climate links is that variations in albedo have unambiguous  
106 climatological impacts, whereas variations in cloud fraction have no such direct  
107 climatological correspondence since they may be compensated for by changes in  
108 optical depth. Few studies have explored the possibility that CRs could influence

109 cloud height, and so we also analyzed cloud heights in addition to albedos in case a  
110 connection has been overlooked.

### 111 **3. Long-Term Analysis**

#### 112 **3.1. Methodology**

113 Global and regional monthly albedos were calculated by weighting each block by  
114 latitude and solar insolation, and the resulting time series were anomalized by  
115 subtracting monthly averages. Latitude weighted monthly cloud height anomalies  
116 were similarly calculated. Orbits were assumed to be independent for the purposes  
117 of calculating the standard error (SE) in albedo or cloud height anomalies for each  
118 time period. To calculate p-values for correlation coefficients, temporal  
119 autocorrelation was accounted for by calculating the effective sample size for each  
120 time series [*Chatfield, 1996*]. Unless otherwise stated  $p < 0.05$  (two-tailed) is taken to  
121 be a statistically significant correlation.

#### 122 **3.2. Results**

123 Fig. 1 shows the global albedo anomaly (continuous red) and the normalized CR  
124 anomaly (dashed blue) for the 13 years of MISR's operation. The correlation  
125 coefficient between the two time series is -0.57. The high degree of autocorrelation  
126 in the CR time series means the effective sample size (3 months) is too small for the  
127 p-value to be meaningful, though it is still not significant. The negative correlation is  
128 largely attributable to the downward trend in global albedo due to sea-ice melt  
129 [*Davies, 2013*] and the apparent upward trend in CRs is due to the chosen start/end

130 point in the 11-year solar cycle (see *Gray et al.* [2010] for recent CR flux increase in  
131 the context of previous solar cycles). If the two time series are detrended then the  
132 correlation coefficient increases to -0.10, the effective sample size increases to 5.3  
133 months and the p-value of the correlation coefficient is 0.86.

134 To test the possibility that monthly variations in the CR flux are correlated with  
135 global albedo, the albedo time series was detrended and the 11-year solar cycle was  
136 removed by subtracting a 3-year running mean from the CR time series. The  
137 resulting time series are shown in the supplementary material (Fig. S1). The  
138 correlation coefficient between the two time series is 0.11, the effective sample size  
139 is 35.6 months and the p-value of the correlation is 0.52. When this analysis was  
140 repeated for cloud-top height there were also no statistically significant correlations  
141 with the CR flux on long timescales (not shown).

142 A lagged correlation was performed between global albedo and normalized CRs  
143 over a  $\pm 600$  day period (Fig. S2). This was done for (a) neither albedos nor CRs  
144 detrended, (b) both time series detrended, and (c) albedos detrended and the 11-  
145 year solar cycle removed from the CR time series as described above. In all three  
146 cases the best correlation occurs for positive lags, which is the non-causal direction  
147 for CRs influencing albedos. We also observe that in all three cases there are no  
148 (causal) lag values for which the correlation is significant, which is consistent with  
149 the null hypothesis.

150 To test for regional CR–cloud connections, albedos were binned by latitude and  
151 longitude and the time series for each grid box was correlated with the (global)

152 normalized CR anomaly. Fig. 2a shows the resulting correlation coefficients as a  
153 function of latitude and longitude, and Fig. 2b shows correlation coefficients as a  
154 function of latitude only (in both cases both time series were detrended). Evidently  
155 there is no obvious spatial structure to the correlations and the vast majority of  
156 correlation coefficients are weak, with 90% falling between -0.37 and 0.37. Note  
157 that if neither time series is detrended (Fig. S3) we observe strong negative  
158 correlations in the arctic attributable to the melt of sea-ice. The Eurasian regions of  
159 negative correlation in Fig. 2a have the wrong sign for mechanisms that amplify TSI  
160 changes, and they disappear when the 11-year solar cycle is removed (Fig. S4). Fig.  
161 2a also shows a slight tendency for positive correlations near the South Pole, but  
162 high latitudes have zero retrievals in winter and the correlations disappear when  
163 the 11-year solar cycle is removed. In short there is no evidence for any regional  
164 connections between CRs and albedos.

## 165 **4. Forbush Decrease Analysis**

### 166 **4.1. Methodology**

167 The Kerguelen Neutron Monitor ( $R=1.14$  GV) was used to represent the global CR  
168 flux for the Fd analysis instead of a normalized eight station composite. 14 Fd events  
169 were chosen for the composite analysis (see supplementary material for list of event  
170 dates). Events were excluded from the composite if secondary Fd of comparable  
171 magnitude were apparent within  $\pm 20$  days of the decrease minima, or if a strong (i.e.  
172  $>2\%$  increase within 1 day) ground level enhancement (GLE) was present within  
173  $\pm 20$  days of the minima. GLEs are brief increases ( $\sim$ hours) in the CR flux that occur



174 when solar CRs cross the path of the Earth. They can be a confounding factor in Fd  
175 analyses since they act to offset coincident Fd events. The 14 Fd events were  
176 averaged by aligning their minima, and the analysis period was chosen to be 53 days  
177 (21 days prior the minima plus 31 following the minima).

178 Given the dates for each Fd, albedo and cloud height data for these dates were  
179 extracted from the MISR level 2 dataset. The 14 albedo time series that correspond  
180 to the Fd events were aligned and superposed in the same way to produce an event-  
181 averaged albedo time series. This was done both globally and regionally. The albedo  
182 time series, cloud height time series and CR time series were anomalized by  
183 subtracting a 21-day running mean. This was done to remove intermediate to long  
184 timescale trends/variability that were unrelated to the influence of sudden CR  
185 decreases (see *Laken and Calogovic* [2013] for further discussion).

186 To evaluate the significance of anomalies within the composite time series, and of  
187 correlations between different time series, Monte Carlo (MC) simulations were run  
188 for all Fd analyses using 14-event composites selected at random from the 13 years  
189 of MISR data. The resulting distributions of anomalies and correlation coefficients  
190 were used to evaluate statistical significance. The MC methodology we implemented  
191 is described in detail by *Laken and Calogovic* [2013].

## 192 **4.2. Results**

193 Fig. 3a shows the superposed CR time series for all 14 Fd events. The SE in the CR  
194 composite is also shown in addition to confidence intervals based on 100,000 MC  
195 simulations ( $p < 0.05$  and  $p < 0.01$  two-tailed levels are plotted). There is a clear

196 statistically significant variation in the CR flux during Fds with 40% of days showing  
197 significant anomalies at the  $p < 0.05$  level. Fig. 3b shows the cotemporal broadband  
198 global albedo anomaly averaged over the same 14 events. There are only four days  
199 with anomalies significant at the  $p < 0.05$  level, and zero days with anomalies  
200 significant at the  $p < 0.01$  level which is consistent with the null hypothesis for a time  
201 series with 53 independent data points. Of the four statistically significant anomalies  
202 one is prior to the CR decrease and therefore non-causal, two have the wrong sign  
203 for the CCN mechanism suggested by *Marsh and Svensmark* [2000] and all four are  
204 only one day in duration, which is indicative of random noise rather than a  
205 sustained cloud response. The brief positive albedo anomaly at  $t = 2$  days is arguably  
206 consistent with a negative-signed global electric circuit mechanism, though the  
207 anomaly is barely larger than the 95% confidence interval and thus difficult to  
208 distinguish from noise. The correlation coefficient between the two time series is -  
209 0.11 and is not significant at the  $p < 0.4$  level. We conclude that there is no detectable  
210 global albedo response to the CR decrease consistent with a TSI-amplifying  
211 mechanism. Furthermore since there is no detectable albedo response larger than  
212 the noise in our composite, then it follows with 95% confidence that if a CR-global  
213 albedo relationship does exist then a 5% decrease in CRs can, at most, alter global  
214 albedo by  $\leq 0.0029$ . The implications of this upper limit are explored in the  
215 discussion below.

216 The analysis described above was repeated using only the five largest Fd events to  
217 test the possibility of a threshold effect (Fig. S5). The analysis was also repeated by  
218 partitioning albedos into land and ocean and examining each time series

219 independently (Fig. S6). In both cases there were no statistically significant  
220 anomalies at the  $p < 0.01$  level within 25 days of the Fd minima, and the total number  
221 of significant anomalies at the  $p < 0.05$  level was consistent with the null hypothesis.  
222 Furthermore none of the correlation coefficients between the composite albedo and  
223 CR anomaly time series were significant at the  $p < 0.4$  level. Note however that  
224 restricting the sample reduces the detectability of albedo responses to CR decreases  
225 (see *Laken and Calogovic* [2013] for further discussion).

226 To test for a latitudinally stratified response, albedo time series for 10 latitude bins  
227 were calculated and compared to the CR composite (Fig. S7). There was nothing to  
228 suggest a latitudinally stratified albedo response to Fds, with only one incidence of  
229 consecutive  $p < 0.05$  anomalies occurring within 30 days of the Fd minima.

230 Fig. 3c shows the average global cloud height time series coincident with the Fd  
231 events in Fig. 3a. There is a highly significant (albeit wrong signed) negative cloud  
232 height anomaly ( $p < 0.0005$ ) 17 days after the Fd minima. However this anomaly is  
233 likely to be spurious because (i) the anomaly disappears completely when the  
234 sample is restricted to the five strongest Fd events (Fig. S9), (ii) it is difficult to  
235 imagine a physical mechanism that would cause global cloud height to sharply  
236 decrease precisely 17 days after Fd minima for only one day in duration, and (iii)  
237 there are no clear altitudinal (Fig. S8) or latitudinal (not shown) responses at 17  
238 days. Assuming the anomaly at 17 days is spurious, the lack of a cloud height  
239 response allows us to conclude with 95% confidence that if a CR–cloud top height  
240 relationship does exist then a 5% decrease in CRs can, at most, alter global average

241 cloud-top height by 60m. Radiative-convective modeling [Davies, 2013] suggests  
242 that a 60m change in effective cloud height would cause a 0.4°C change in surface  
243 temperature.

## 244 **5. Discussion**

245 Long-term analysis of 13 years of MISR data reveals no statistically significant  
246 correlations between the CR flux and global albedo or globally averaged cloud  
247 height on monthly or interannual timescales. Additionally there are no statistically  
248 significant lagged correlations, and no evidence for any regional correlations.

249 Epoch superposition of 14 Fd events also reveals no evidence for any albedo or  
250 cloud height response to decreases in the CR flux on daily to weekly timescales.  
251 Stratifying data by latitude, surface type and restricting analysis to only the largest  
252 Fds does not reveal any significant albedo responses inconsistent with the null  
253 hypothesis. In this case we can use the null result to constrain the maximum  
254 possible influence of CRs on global albedo, and find that if a CR–global albedo  
255 relationship does exist then a 5% decrease in the CR flux can, at most, alter global  
256 broadband albedo by  $\leq 0.0029$ .

257 Given this result we can ask the question: if the CR modulation of global albedo was  
258 responsible for recent global warming, would we expect to see a signal in our global  
259 albedo composite (Fig. 3b) given the magnitude of the Fds and the noise in our data?  
260 The observed increase in global average surface temperature since 1900 is around  
261 0.8°C [Hansen *et al.*, 2010]. If we assume a conservative climate sensitivity to global

262 albedo changes of  $\lambda = 0.5^{\circ}\text{C}/(\text{Wm}^{-2})$ , then it follows that the necessary secular  
263 change in albedo to explain global warming since 1900 is 0.0047. The observed  
264 decrease in the CR flux since 1891 is  $-5.2 \pm 1.6\%$  (Fig. S10). Thus to explain  
265 observed global warming via CR modulation of albedos it is necessary to postulate  
266 that a 5% decrease in the CR flux decreases global albedo by around half a percent.  
267 Fortuitously the secular decrease in the CR flux since 1891 is equal to the average Fd  
268 magnitude in our composite analysis. Thus if CR flux decreases were responsible for  
269 recent warming then an albedo signal should be visible in our Fd analysis since the  
270 95% confidence interval extends to only 0.0029. Instead we observe that there is no  
271 global albedo response to a 5% decrease in CRs greater than 0.0029 and no hint of  
272 any weaker signals imbedded in the noise either. We note that this approach  
273 understates the case for expecting to detect an albedo response since (i) the 21-day  
274 running mean subtraction tends to reduce the magnitude of Fds by 1-2%, (ii) the  
275 cutoff rigidity of the CR monitor used in Fd analysis ( $R=1.14$  GV) is slightly greater  
276 than the cutoff rigidity of the CR reconstruction used to determine long term trends  
277 ( $R=0.8$  GV), and (iii) since Fds last several days we expect any albedo response to  
278 similarly last more than a day, but p-values have been calculated assuming  
279 independent daily anomalies (in other words the probability of there being a  
280 sustained albedo response of a given magnitude hidden within the noise diminishes  
281 as the expected response time increases). Although our conservative value for  
282 climate sensitivity arguably overstates the case for detectability, we believe such a  
283 choice is justified for two reasons. Firstly if sensitivity were high then the climate  
284 system would not yet be in equilibrium and thus using the full sensitivity would be

285 misleading, and secondly, a high sensitivity to radiative forcings contradicts the  
286 starting assumption that cosmic rays are responsible for recent warming; if  
287 sensitivity were high then 20<sup>th</sup> century greenhouse gas increases would have caused  
288 observed warming contrary to this assumption. It should also be noted that the  
289 secular trend in CRs in the last 50 years (in which time 0.6°C of warming has  
290 occurred) is 1.4%. This trend is of the wrong sign and 4.4 times too small to explain  
291 recent warming given the 95 percentile upper limit on the CR influence from Fig. 3b.  
292 The analysis above suggests that CR modulation of albedo is not responsible for the  
293 majority of global warming since 1900.

294 One caveat on these conclusions is that the upper bound of 0.0029 per 5% CR  
295 decrease was derived exclusively in the context of short timescale Fds. It is  
296 conceivable that CRs influence climate via some unknown mechanism that only acts  
297 on longer timescales, and thus wouldn't be apparent during brief Fd episodes.  
298 However the majority of CR mechanisms proposed in the literature would be  
299 expected to manifest themselves on short timescales since the effects of CRs on  
300 atmospheric ionization are immediate, and cloud-formation processes operate on  
301 the order of hours to days.

302 Although both short and long term analysis did not uncover any evidence for  
303 spatially localized CR–cloud correlations, local effects cannot be dismissed because  
304 the grid size of block-averaged MISR data is large and the sampling errors in  
305 regional correlations are too large to tightly constrain the magnitude of local effects.

306 **Acknowledgements.** We sincerely thank Benjamin A. Laken (Instituto de  
307 Astrofísica de Canarias), Abhnil A. Prasad (UNSW) and the two anonymous  
308 reviewers for their many helpful comments. We acknowledge the NMDB database  
309 founded under the European Union's FP7 program for providing data. Kerguelen  
310 neutron monitor data were kindly provided by the French Polar Institute and by  
311 Paris Observatory. The original MISR datasets were obtained from the NASA  
312 Langley Research Center Atmospheric Science Data Center.

### 313 **References**

- 314 Bazilevskaya, G. A., et al. (2008), Cosmic ray induced ion production in the  
315 atmosphere. *Space Sci. Rev.*, 137(1-4), 149-173.
- 316 Bond, G., et al. (2001), Persistent solar influence on north Atlantic climate during the  
317 Holocene. *Science*, 294(5549), 2130-2136.
- 318 Calogovic, J., et al. (2010), Sudden cosmic ray decreases: No change of global cloud  
319 cover. *Geophys. Res. Lett.*, 37, doi:10.1029/2009gl041327
- 320 Chatfield, C. (1996), The analysis of time series: An introduction, 5<sup>th</sup> ed., pp. 21-25.,  
321 Chapman and Hall, London.
- 322 Damon, P. E., and P. Laut (2004), Pattern of Strange Errors Plagues Solar Activity  
323 and Terrestrial Climate Data. *Eos Trans. AGU*, 85(39), 370-374,  
324 doi:10.1029/2004eo390005

- 325 Davies, R. (2013), Comparison of Longwave and Shortwave Cloud Effects on  
326 Equilibrium Surface Temperature using a Radiative-Convective Model and 12 Years  
327 of MISR Observations, *Radiation Processes in the Atmosphere and Ocean (IRS2012)*,  
328 AIP Conf. Proc. 1531, 720-723.
- 329 Diner, D. J., et al. (1999), MISR Level 2 Top-of-Atmosphere Albedo Algorithm  
330 Theoretical Basis. *Jet. Propul. Lab.*, Pasadena, Calif.
- 331 Gray, L. J., et al. (2010), Solar influences on climate. *Rev. Geophys.*, 48,  
332 doi:10.1029/2009rg000282
- 333 Haigh, J. D. (1996), The impact of solar variability on climate. *Science*, 272(5264),  
334 981-984.
- 335 Hansen, J., R. Ruedy, M. Sato, and K. Lo (2010), Global surface temperature change.  
336 *Rev. Geophys.*, 48, doi:10.1029/2010RG000345.
- 337 Jorgensen, T. S., and A. W. Hansen (2000), Comments on "Variation of cosmic ray  
338 flux and global cloud coverage - a missing link in solar-climate relationships" by H.  
339 Svensmark and E. Friis-Christensen. *J. Atmos. Sol-Terr. Phy.*, 62(1), 73-77.
- 340 Kirkby, J. (2007), Cosmic rays and climate. *Surv. Geophys.*, 28(5-6), 333-375,  
341 doi:10.1007/S10712-008-9030-6
- 342 Kristjánsson, J. E., J. Kristiansen and E. Kaas (2004), Solar activity, cosmic rays,  
343 clouds and climate - an update. *Adv. Space. Res.*, 34(2), 407-415,  
344 doi:10.1016/j.asr.2003.02.040

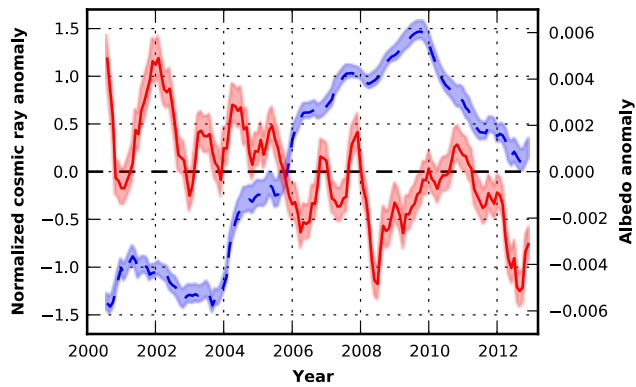


- 345 Kristjansson J. E., et al. (2008), Cosmic rays, cloud condensation nuclei and clouds –  
346 a reassessment using MODIS data. *Atmos. Chem. Phys.*, 584 8(24), 7373–7387.
- 347 Laken, B., and J. Calogovic, (2011), Solar irradiance, cosmic rays and cloudiness over  
348 daily timescales. *Geophys. Res. Lett.*, 38, doi:10.1029/2011gl049764
- 349 Laken, B., D. Kniveton and A. Wolfendale (2011), Forbush decreases, solar irradiance  
350 variations, and anomalous cloud changes. *J. Geophys. Res-Atmos.*, 16,  
351 doi:10.1029/2010jd014900
- 352 Laken, B., E. Palle, J. Calogovic, and E. Dunne (2012), A cosmic ray-climate link and  
353 cloud observations. *J. Space Weather Space Clim.*, 2(A18), 13.
- 354 Laken, B. and J. Calogovic (2013), Composite analysis with Monte Carlo method: an  
355 example with cosmic rays and clouds. *J. Space Weather Space Clim.*, in press,  
356 doi:10.1051/swsc/2013051
- 357 Marsh, N., and H. Svensmark (2000), Cosmic rays, clouds, and climate. *Space Sci. Rev.*,  
358 94(1-2), 215-230.
- 359 Marsh, N., and H. Svensmark (2003), Solar influence on Earth's climate. *Space Sci.*  
360 *Rev.*, 107(1-2), 317-325.
- 361 Meehl, G. A., J. M. Arblaster, K. Matthes, F. Sassi, and H. van Loon (2009), Amplifying  
362 the pacific climate system response to a small 11-year solar cycle forcing. *Science*,  
363 325(5944), 1114-1118, doi:10.1126/Science.1172872

- 364 Neff, U., et al. (2001), Strong coherence between solar variability and the monsoon  
365 in Oman between 9 and 6 kyr ago. *Nature*, 411(6835), 290-293.
- 366 Pallé, E., and C. J. Butler (2000), The Influence of cosmic rays on terrestrial cloud and  
367 global warming. *Astron. Geophys.*, 41, 4.18-4.22
- 368 Pudovkin, M. and S. Veretenenko (1995), Cloudiness decreases associated with  
369 Forbush-decreases of galactic cosmic rays. *J. Atmos. Terr. Phys.*, 57(11), 1349-1355
- 370 Rao, U. R. (2011), Contribution of changing galactic cosmic ray flux to global  
371 warming. *Curr. Sci. India.*, 100 (2), 223-225.
- 372 Sloan, T., and A. W. Wolfendale (2008), Testing the proposed causal link between  
373 cosmic rays and cloud cover. *Environ. Res. Lett.*, 3(2).
- 374 Sun, B. M. and R. S. Bradley (2002), Solar influences on cosmic rays and cloud  
375 formation: A reassessment. *J. Geophys. Res-Atmos.* 107(D14),  
376 doi:10.1029/2001jd000560
- 377 Svensmark, H. (2007), Cosmoclimatology: A new theory emerges. *Astron. Geophys.*,  
378 48(1), 18-24.
- 379 Svensmark, H., and E. Friis-Christensen (1997), Variation of cosmic ray flux and  
380 global cloud coverage - A missing link in solar-climate relationships. *J. Atmos. Sol-  
381 Terr. Phys.*, 59(11), 1225-1232.

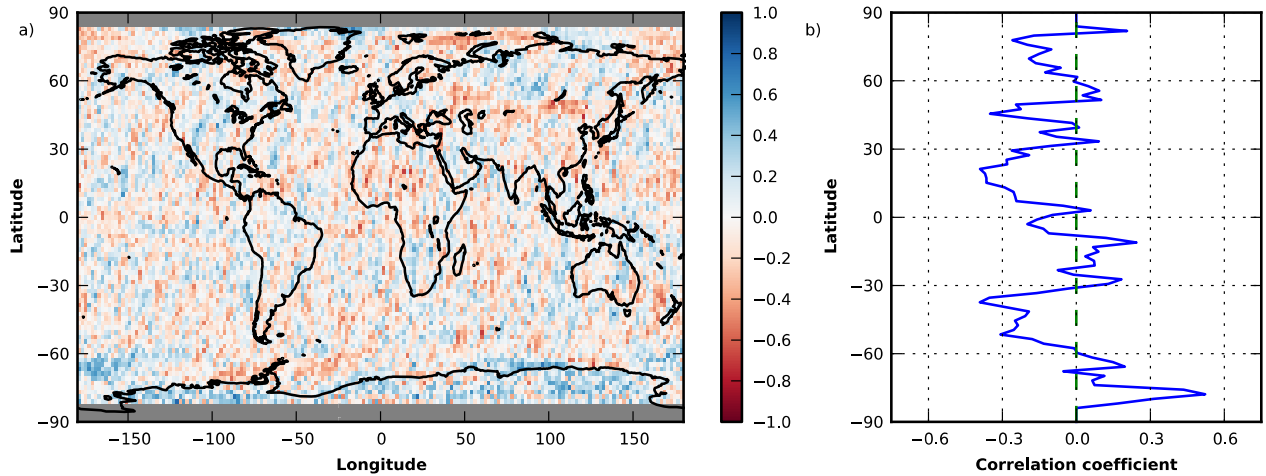
- 382 Svensmark, J., M. Enghoff, and H. Svensmark (2012), Effects of cosmic ray decreases  
383 on cloud microphysics, *Atmos. Chem. Phys. Discuss.*, 12, 3595–3617, doi:  
384 10.5194/acpd-12-3595-2012
- 385 Tinsley, B. (2008), The global atmospheric electric circuit and its effects on cloud  
386 microphysics. *Rep. Prog. Phys.*, 71 (6), 066801.
- 387 Todd, M. C., and D. R. Kniveton (2001), Changes in cloud cover associated with  
388 Forbush decreases of galactic cosmic rays. *J. Geophys. Res-Atmos.*, 106(D23), 32031-  
389 32041.
- 390 Todd, M. C., and D. R. Kniveton (2004), Short-term variability in satellite-derived  
391 cloud cover and galactic cosmic rays: an update. *J. Atmos. Sol-Terr. Phy.*, 66(13),  
392 1205–1211.

393 **Figures**

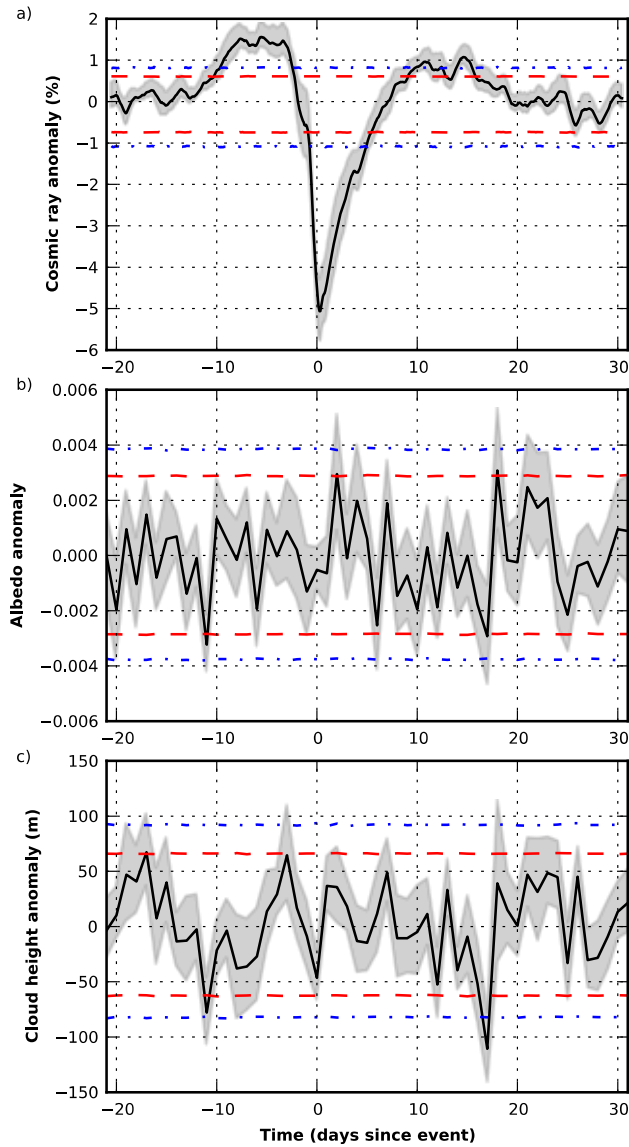


394

395 *Figure 1.* Normalized CR anomaly (dashed blue line) and global albedo anomaly  
 396 (continuous red line) plotted as a function of time. Albedos were retrieved in the  
 397 green channel (558nm) and both time series were smoothed using a flat 7-month  
 398 window, though results were robust to changes in the smoothing window and  
 399 wavelength. Shaded confidence intervals denote  $\pm 1$  SE.



400  
401 *Figure 2.* (a) Correlation coefficient between albedo and normalized CR anomalies as  
402 a function of latitude and longitude ( $1^\circ$  by  $1^\circ$  resolution). (b) Correlation coefficient  
403 as a function of latitude ( $1^\circ$  zonal bands). Albedos were retrieved in the green  
404 channel (558nm) and both time series were smoothed using a flat 7-month window,  
405 though results were robust to changes in the smoothing window and wavelength.  
406 Both time series have been detrended.



407

408 *Figure 3.* Composite time series averaged over all 14 Fd events as a function of days  
 409 since the Fd minima. Subfigures denote (a) CR anomaly, (b) the corresponding  
 410 (broadband) global albedo anomaly, and (c) the average global cloud height  
 411 anomaly. Grey shaded regions denote  $\pm 1$  SE. Red dashed lines show the limits of the  
 412 95% confidence interval and blue dash-dotted lines show the limits of the 99%  
 413 confidence interval based on 100,000 MC simulations. The average values for

414 confidence intervals are (a) red -0.74 to 0.61 and blue -1.09 to 0.82, (b) red -0.0028  
415 to 0.0029 and blue -0.0038 to 0.0038, and (c) red -62.5 to 66.1 and blue -82.2 to 92.3.

## Auxiliary Material 1: Supplementary figures

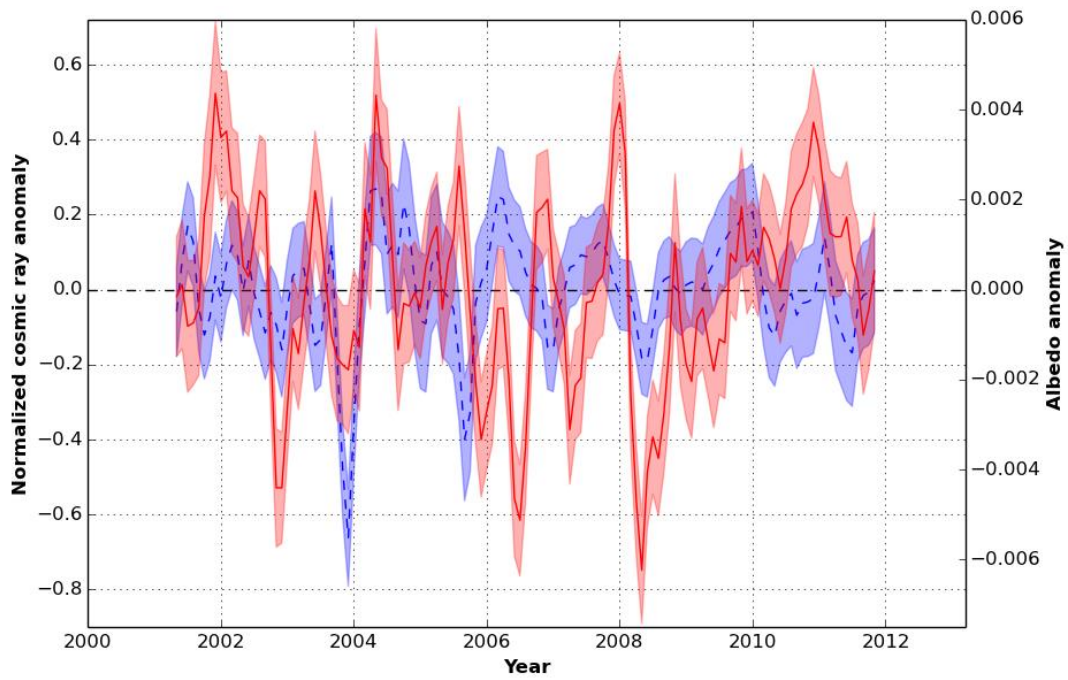


*Figure S1.* Normalized cosmic ray anomaly (dashed blue line) with solar cycle removed as described in main text and detrended global albedo anomaly (continuous red line) plotted as a function of time. Albedos were retrieved in the green channel (558nm) and both time series were smoothed using a flat 3-month window. Shaded confidence intervals denote  $\pm 1$  standard error.



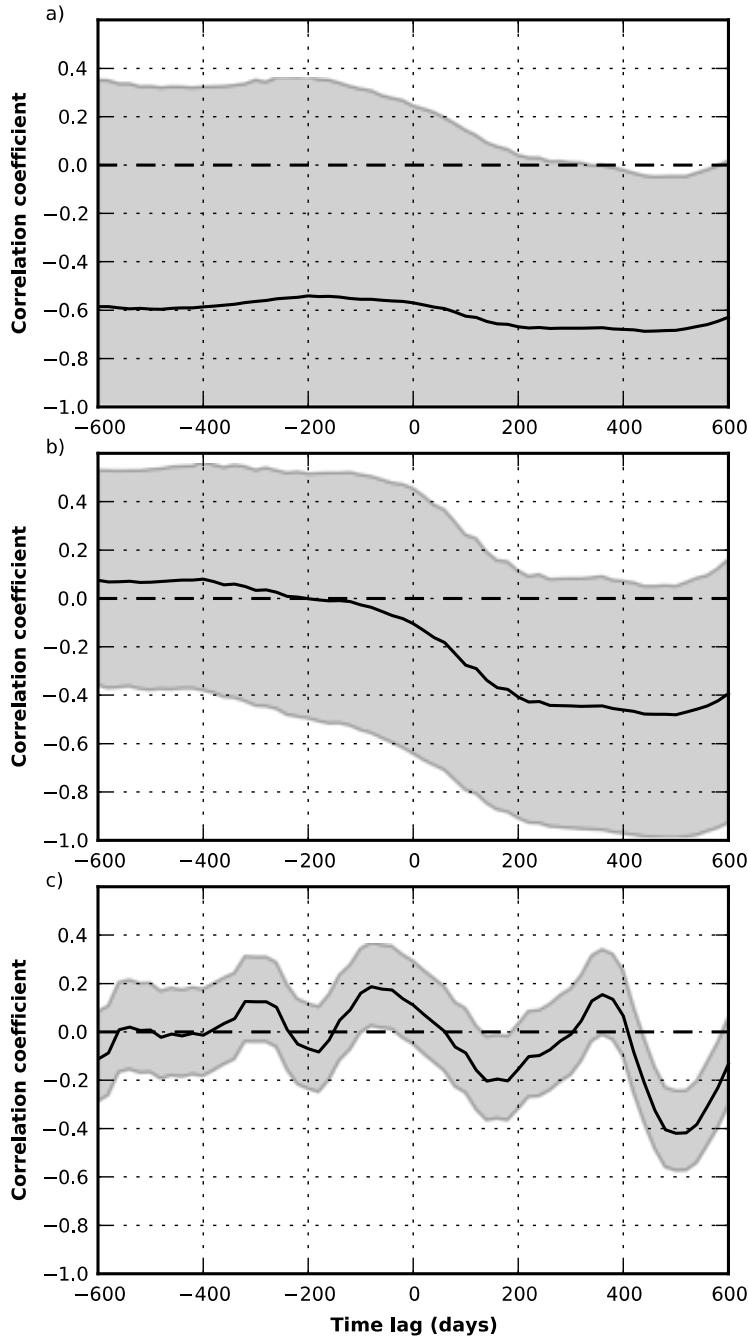


*Figure S2.* Correlation coefficient between global albedo and normalized cosmic ray anomaly as a function of lag for (a) neither time series detrended, (b) both albedo and cosmic rays detrended, and (c) albedos detrended and solar cycle removed from cosmic rays. A positive lag denotes cosmic rays leading albedos (i.e. cosmic rays pushed backwards in time). Grey shading represents  $\pm 1$  SE. Note that the errors are larger for (a) and (b) due to strong autocorrelation in the cosmic ray time series.

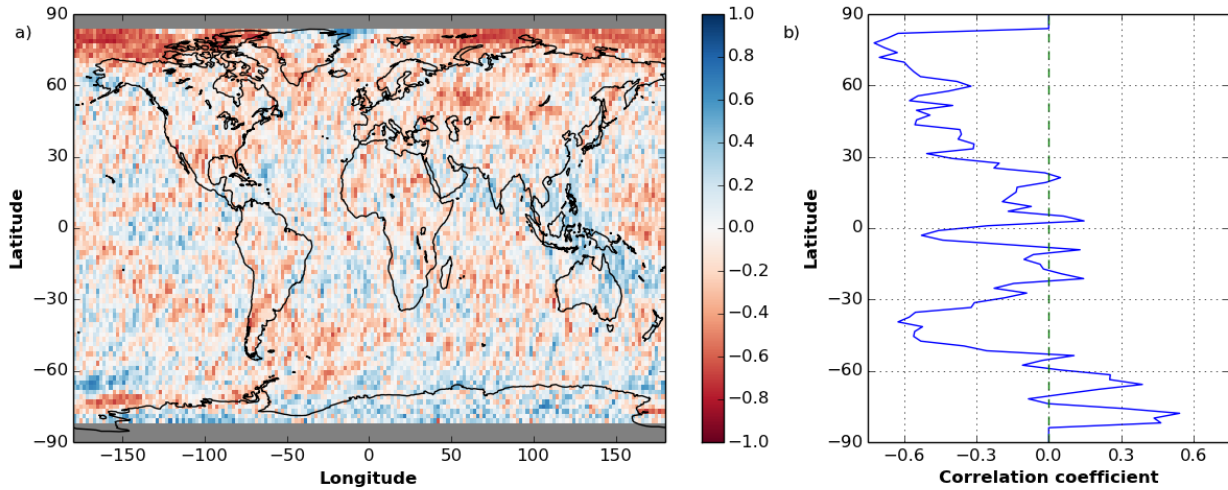


Figure S3. (a) Correlation coefficient between albedo and normalized cosmic ray anomalies as a function of latitude and longitude ( $1^\circ$  by  $1^\circ$  resolution). (b) Correlation coefficient as a function of latitude ( $1^\circ$  zonal bands). Albedos were retrieved in the green channel (558nm) and both time series were smoothed using a flat 7-month window. Neither time series was detrended. The weaker spatial structures in this figure closely resemble the SOI correlations in *Davies and Molloy* [2012].

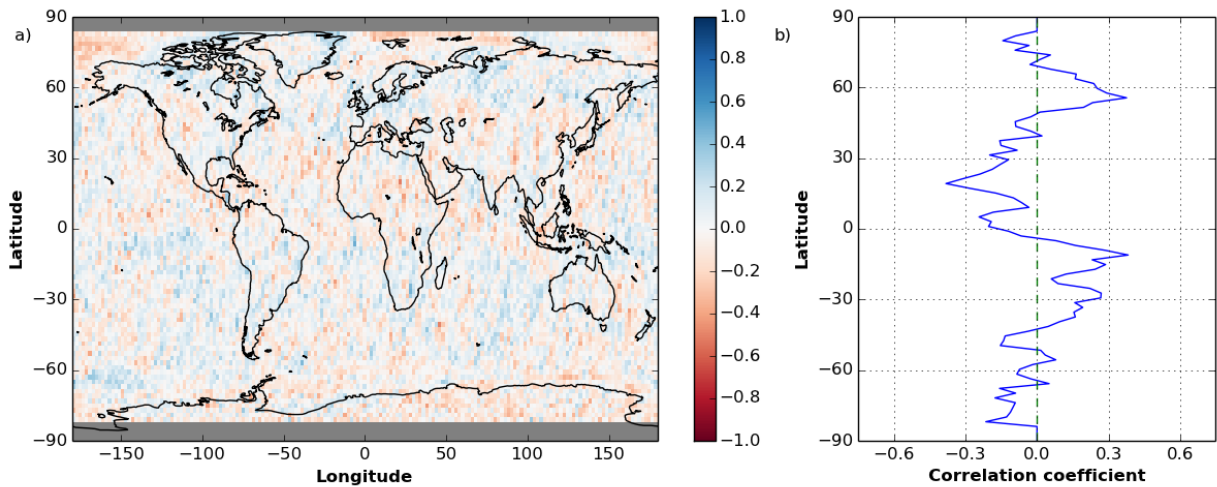
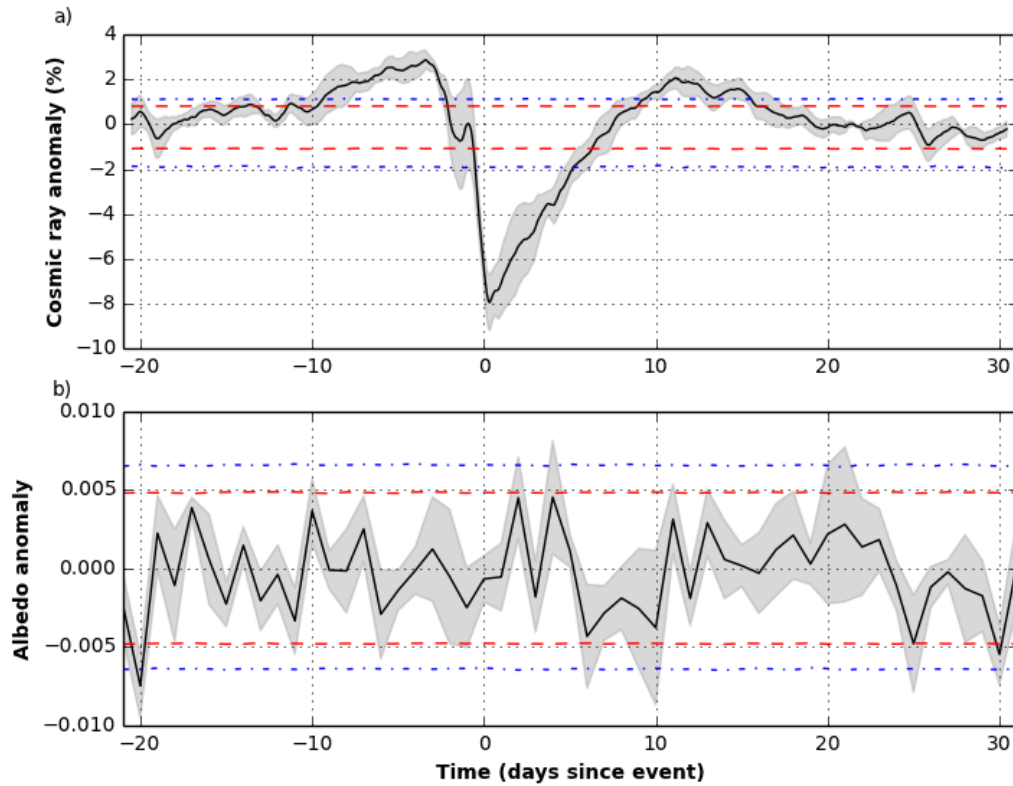
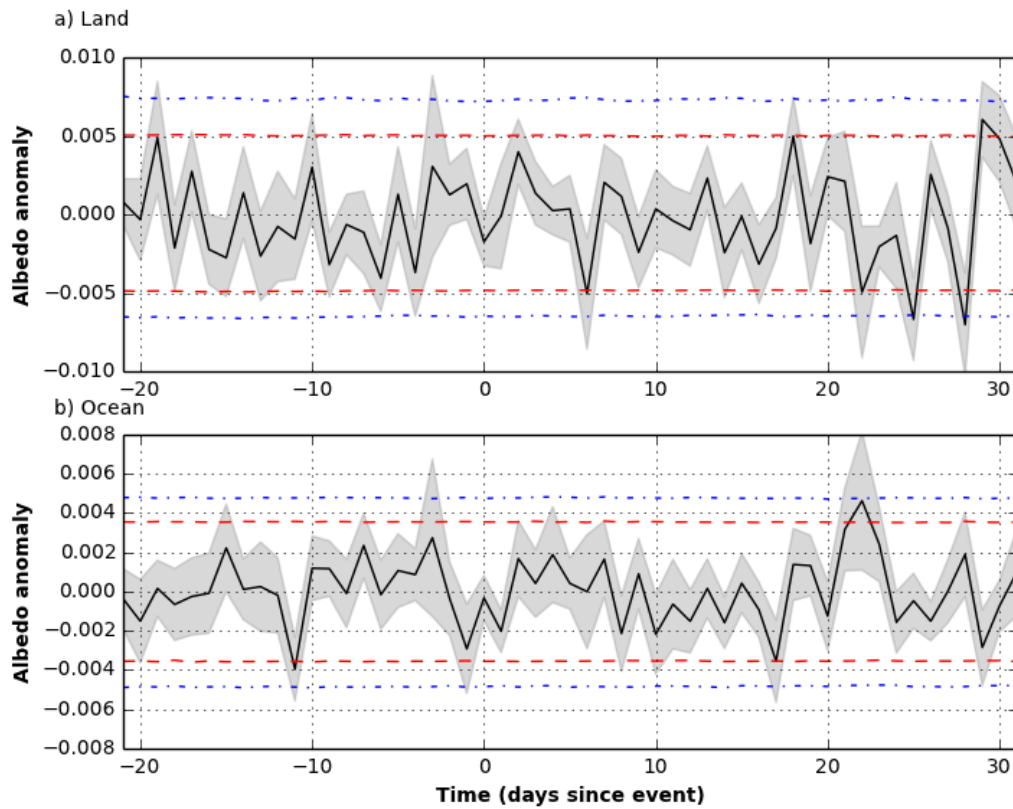


Figure S4. (a) Correlation coefficient between albedo and normalized cosmic ray anomalies as a function of latitude and longitude ( $1^\circ$  by  $1^\circ$  resolution). (b) Correlation coefficient as a function of latitude ( $1^\circ$  zonal bands). Albedos were retrieved in the green channel (558nm) and both time series were smoothed using a flat 3-month window. Albedos have been detrended and solar cycle has been removed from cosmic rays.



*Figure S5.* Identical to Fig. 3a and Fig. 3b respectively in the main text except analysis restricted to only the five largest Fd events. Grey shaded regions denote  $\pm 1$  SE. Red dashed lines show the limits of the 95% confidence interval and blue dash-dotted lines show the limits of the 99% confidence interval based on 100,000 MC simulations. The average values for confidence intervals are (a) red -1.09 to 0.81 and blue -1.91 to 1.12, and (b) red -0.0047 to 0.0048 and blue -0.0064 to 0.0066.



*Figure S6.* Identical to Fig. 3b in the main text except albedo retrievals partitioned into (a) above-land and (b) above-ocean. All 14 Fd events have been used to build these composites. Grey shaded regions denote  $\pm 1$  SE. Red dashed lines show the limits of the 95% confidence interval and blue dash-dotted lines show the limits of the 99% confidence interval based on 100,000 MC simulations. The average values for confidence intervals are (a) red -0.0048 to 0.0050 and blue -0.0065 to 0.0073, and (b) red -0.0035 to 0.0035 and blue -0.0048 to 0.0048.

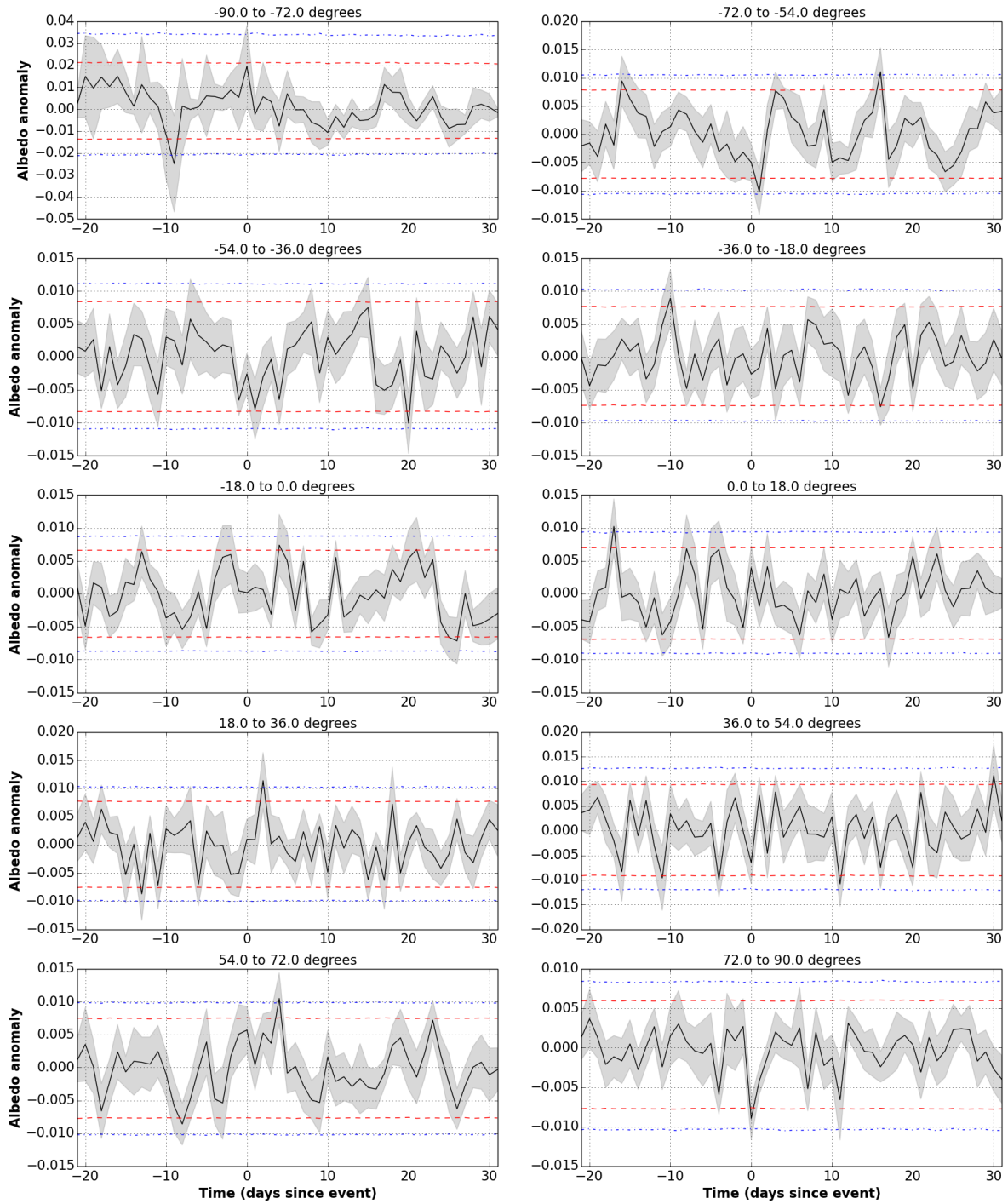


*Figure S7.* Each subfigure shows the composite (broadband) albedo time series for a different latitude band averaged over all 14 Fd events. 4% of the anomalies in all the time series are significant at the  $p < 0.05$  level which is consistent with the null hypothesis. Grey shaded regions denote  $\pm 1$  SE. Red dashed lines show the limits of the 95% confidence interval and blue dash-dotted lines show the limits of the 99% confidence interval based on 100,000 MC simulations. The average values of

confidence intervals are (red interval then blue interval from negative to positive latitudes): -0.013 to 0.021, -0.021 to 0.034; -0.0078 to 0.0079, -0.011 to 0.011; -0.0083 to 0.0084, -0.011 to 0.011; -0.0074 to 0.0077, -0.0097 to 0.010; -0.0066 to 0.0066, -0.0087 to 0.0088; -0.0069 to 0.0071, -0.0091 to 0.0094; -0.0075 to 0.0077, -0.0099 to 0.010; -0.0091 to 0.0094, -0.012 to 0.013; -0.0077 to 0.0075, -0.010 to 0.0099; -0.0077 to 0.0060, -0.010 to 0.0084.

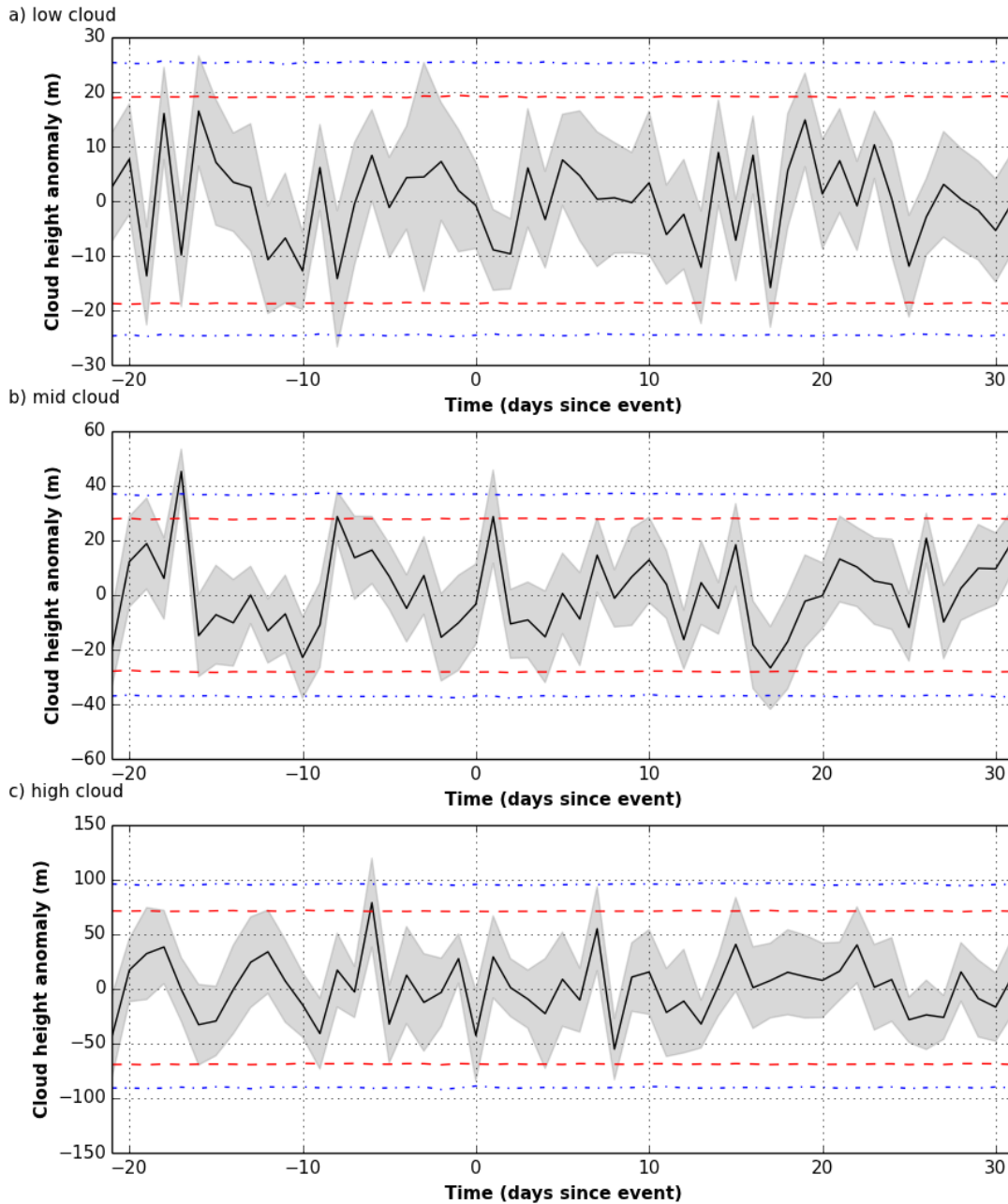
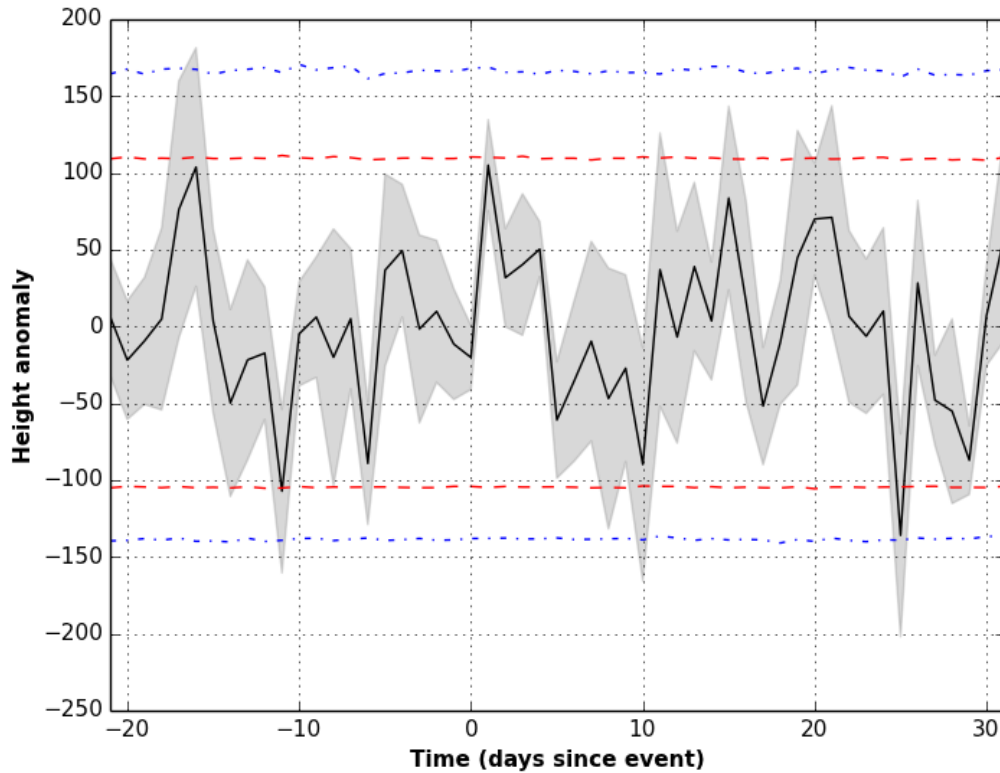


Figure S8. Average global cloud height response to 14 Fd events for (a) low, (b) middle and (c) high level cloud. Confidence intervals and standard errors denoted as above. We note that there is no statistically significant anomaly in low, middle or high cloud at  $t=17$  days. The average values for confidence intervals are (a) red -18.6 to 19.1 and blue -24.5 to 25.4, (b) red -28.0 to 27.9 and blue -37.0 to 36.9, and (c) red -68.9 to 71.1 and blue -90.4 to 95.5. *Harrison et al.* [2011] reports a change in the cloud base anomaly distribution when comparing high and low neutron count terciles. It is difficult to directly compare this result to our findings due to uncertainties in how changes in cloud base height translate to cloud top height, and

differences in methodology. However we note that Fig. S8a precludes a global low cloud top response of more than 19m per 5% decrease in the cosmic ray flux.





*Figure S9.* Identical to Fig. 3c in the main text except analysis restricted to only the five largest Fd events. Grey shaded regions denote  $\pm 1$  SE. Red dashed lines show the limits of the 95% confidence interval and blue dash-dotted lines show the limits of the 99% confidence interval based on 100,000 MC simulations. Note how the significant anomaly at  $t=17$  days is now absent. The average values for confidence intervals are red -104.6 to 109.6 and blue -138.5 to 166.4.

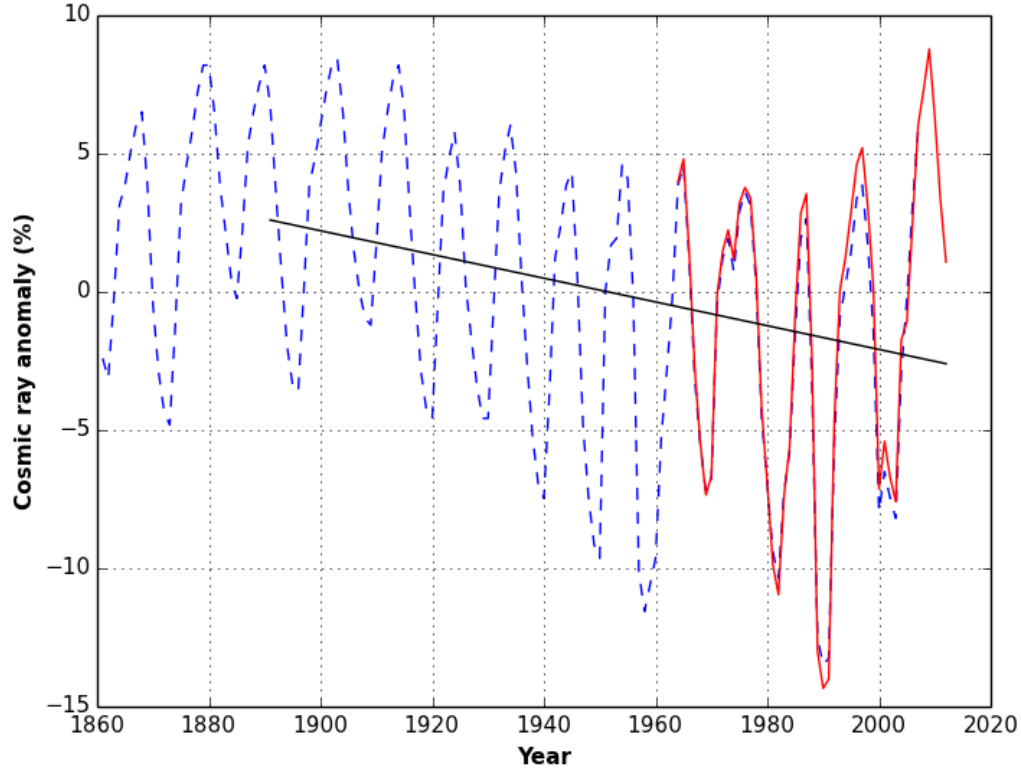


*Figure S10.* Blue dashed line is historical cosmic ray reconstruction from *Usoskin et al.* [2002] for a neutron monitor with rigidity  $R=0.8$  GV, red continuous line is NMBD neutron monitor data from Oulu monitoring station ( $R=0.8$  GV) and the black continuous line shows the secular trend in cosmic rays from 1891 to present (11 complete solar cycles) using the combination of these two time series. The overall change since 1891 is  $-5.2 \pm 1.6\%$ . The error in the trend was calculated assuming zero autocorrelation, though if autocorrelation is accounted for then (depending on methodology) the trend may not be statistically significant.

## Cosmic Ray Data

### Long term analysis:

Cosmic ray data were retrieved from the Neutron Monitoring Database (NMDB, [www.nmdb.eu](http://www.nmdb.eu)). 8 different NMDB cosmic ray monitoring stations were used to build cosmic ray composite time series that represented the global flux for the 13 years of MISR's operation. Each individual time series was anomalized, scaled by its own variance and averaged to produce a 13-year cosmic ray composite as described in main text. Averaging the cosmic ray flux from multiple stations isn't strictly necessary since all stations are very closely correlated with one another, however it does help smooth out minor local variations to better represent the globally averaged surface flux. The stations used were as follows:

Alma-Ata B (R=6.69 GV), AATB  
Rome (R=6.27 GV), ROME  
IGY Jungfrauoch (R=4.49 GV), JUNG  
NM64 Jungfrauoch (R=4.49 GV), JUNG1  
Kiel (R=2.36 GV), KIEL  
Kerguelen (R=1.14 GV), KERG  
Oulu (R=0.81 GV), OULU  
Apatity (R=0.65 GV), APTY

### Short term analysis:

Only the Kerguelen station (R=1.14 GV) in the French Southern and Antarctic Lands was used in the Fd analysis. This was to ensure the percentage variations in the cosmic ray flux could easily be compared to the magnitude of variations on decadal timescales as measured by the Usoskin et. al. (2002) reconstruction (R=0.8 GV). The cosmic ray time series had 2-hourly resolution but was smoothed and interpolated appropriately to match daily sampling in the albedo time series.

### 14 Forbush decrease events used in epoch superposition analysis:

9/6/2000  
18/9/2000  
29/11/2000  
26/9/2001\*  
23/3/2002  
18/4/2002  
31/5/2003  
29/10/2003\*  
15/9/2004  
10/11/2004\*  
12/9/2005\*  
4/8/2010  
18/2/2011  
8/3/2012\*

\* denotes 5 largest events used in sub-sample analysis

The analysis period was chosen to be 53 days; 21 days prior to the minima plus 31 days after the minima plus the minima itself. Arnold (2006) suggests ~7 days as the maximum possible atmospheric response time to CR-induced ionization. The recovery time of Forbush decreases is generally several days. Thus the analysis period was chosen to be several times longer than these events to ensure any signals are clearly distinguishable from background noise (i.e. to provide a clear baseline to contrast with any cosmic ray response).